Available online at www.eccomasproceedia.org
Eccomas Proceedia SMART (2023) 1018-1028

ECCOMAS
Proceedia

X ECCOMAS Thematic Conference on Smart Structures and Materials
SMART 2023
D.A. Saravanos, A. Benjeddou, N. Chrysochoidis and T. Theodosiou (Eds)

NEW QUASI-PHASE-MATCHING TECHNIQUES ENHANCING THE SECOND HARMONIC INTENSITY IN LAMB WAVES– SMART 2023

XIAOQIANG SUN * †

* Chongqing Industry Polytechnic College (CQIPC)
Chongqing 401120, PR China
e-mail: sunxq@cqipc.edu.cn

Abstract. About nonlinear Lamb waves, most previous studies point out that the intensity of the second harmonic is generally low due to the deterioration of phase-velocity matching conditions. In this paper, to enhance the second harmonic intensity, a new technique were put forward based on quasi-phase-matching (QPM). And the material quasi-phase-matching technique (MQPM) for the second harmonic generation in Lamb waves with quadratic nonlinearity by periodically changing the sign of the third-order elastic constants in one-dimensional composite thin plates is proposed. Theoretical and numerical results show that the energy of the second harmonic Lamb wave could be enhanced by using this novel technique. MQPM is straightforward to implement in the experiments.

Keywords: Lamb waves, the second harmonic, quasi-phase-matching, third-order elastic constants.

1 INTRODUCTION

Quasi-phase-matching (QPM) is an old and classical conception. In 1962, shortly after the first nonlinear optical experiment, the interactions between light waves in a nonlinear dielectric were studied. Three kinds of experimental structures have been proposed by Armstrong [1] and his coworker, a Nobel Laureate, Bloembergen, to provide phase correction in case that the phase velocity of the interacting waves is not perfectly matched. Thousands of related studies had been conducted in the nonlinear optical field since then. Nowadays, QPM for a higher-order harmonic generation has been extensively theorized and experimentally studied in optical nonlinear conversion processes [2-9].

Similarly, this QPM technique for a higher-order harmonic generation with the ultrasonic Lamb wave has been also reported. When an ultrasonic Lamb wave propagates through an elastic plate with quadratic nonlinearity, the second-harmonic generation (SHG) will take place [10-16]. It is well known that two conditions, i.e., phase velocity matching and non-zero power flux, are necessary for the cumulative SHG [10-13,15,17]. It is known that the amplitudes of the second harmonics generated increase with the propagation distance in the form of sine functions and exhibit a maximum cumulative propagation distance due to π

Peer-review under responsibility of the organizing committee of SMART 2023.
doi: 10.7712/150123.9853.450221

effects [12,16] caused by the deterioration of phase-velocity matching conditions [10-19], which is a similar phenomenon (phase mismatching) in nonlinear optics. By employing the QPM technique, the intensity of the second harmonic generated can be continuously maintained, and the limitations of the phase velocity matching conditions can be overcome in Lamb waves.

Two QPM-based techniques have been reported till now. The first QPM-based technique is to choose mode pairs that satisfy strict phase-velocity matching criterion (to obtain a linearly increased second harmonic) [18]. However, as stated in the literature [18], some limitations exist. Exact phase-velocity matching is impossible in the whole frequency bandwidth and the number of isolated mode pairs is quite limited. To solve these problems, another QPM-based technique selecting S0 mode at a low-frequency range (which satisfies approximate phase-velocity matching) was employed [18]. However, this technique is limited to a low-frequency range. These two QPM-based techniques failed in the whole frequency bandwidth. For any given frequency, to ensure that the intensity of the generated second harmonic Lamb waves can be continuously maintained, new QPM-based techniques are needed.

In this work, based on theoretical models and numerical simulations, the author proposed and validated a new QPM-based techniques, which can be employed to overcome the mismatch between the phase velocities of the fundamental and second harmonic waves to enhance the intensity of the second harmonic in the whole frequency bandwidth. This method was named the material quasi-phase-matching technique (MQPM), which needs to periodically change the sign of the third-order elastic constant in one-dimensional thin plates.

2 THEORY

To begin, let us consider a finite-amplitude wave propagating in an isotropic and homogeneous plate with stress-free surfaces (Lamb wave). For simplicity, it is assumed that the wave propagates in the x_1-direction and the particles move only in the x_1-x_3 plane. Geometrical and weak material nonlinearities are theoretically considered, and the total displacement field is assumed to be the sum of a primary wave $\mathbf{u}_{(1)}$ (at the frequency ω) and a second harmonic wave $\mathbf{u}_{(2)}$ (at the frequency 2ω) based on the perturbation condition $\left\|\mathbf{u}_{(2)}\right\| << \left\|\mathbf{u}_{(1)}\right\|$. The perturbation method is widely used to solve nonlinear motion equations for harmonic generation in a waveguide. Solutions for the second harmonic by primary Lamb wave propagation are obtained using modal decomposition. This procedure originally assumes that the nonlinearly-generated secondary wave fields (perturbation solution) can be expressed as a superposition of the Lamb wave modes since an orthogonality exists between different Lamb wave modes [12,13,15,17].

Following Lima *et al*. [12,13,15,17], the corresponding nonlinear wave equation for an isotropic and homogeneous plate with a thickness of 2*h* is written as

$$\begin{aligned} &(\lambda+2\mu)\nabla\nabla\cdot[\mathbf{u}]-\mu\nabla\times\nabla\times\mathbf{u}+\nabla\cdot[\mathbf{T}^{NL}(\mathbf{H})]=\rho\ddot{\mathbf{u}}\,, \\ &[\mathbf{T}(\mathbf{H})\cdot\mathbf{n}_3]\big|_{x_3=\pm h}=[\mathbf{T}^{L}(\mathbf{H})\cdot\mathbf{n}_3+\mathbf{T}^{NL}(\mathbf{H})\cdot\mathbf{n}_3]\big|_{x_3=\pm h}=\mathbf{0}\,, \end{aligned} \tag{1}$$

where,

$$\begin{aligned}
&\mathbf{T}(\mathbf{H}) = \mathbf{T}^{L}(\mathbf{H}) + \mathbf{T}^{NL}(\mathbf{H}), \qquad \mathbf{T}^{L}(\mathbf{H}) = \mathbf{S}^{L} = \lambda tr(\mathbf{H})\mathbf{I} + \mu(\mathbf{H} + \mathbf{H}^{T}),\\
&\mathbf{T}^{NL}(\mathbf{H}) = \frac{\lambda}{2} tr(\mathbf{H}^{T}\mathbf{H})\mathbf{I} + \mathscr{C}[tr(\mathbf{H})]^{2}\mathbf{I} + \mathscr{B}\, tr(\mathbf{H})\mathbf{H}^{T} + \frac{\mathscr{A}}{4}(\mathbf{H}^{T})^{2}\\
&+ \frac{B}{2} tr(\mathbf{H}^{2} + \mathbf{H}^{T}\mathbf{H})\mathbf{I} + (\lambda + \mathscr{B}) tr(\mathbf{H})\mathbf{H} + (\mu + \frac{\mathscr{A}}{4})(\mathbf{H}^{2} + \mathbf{H}^{T}\mathbf{H} + \mathbf{H}\mathbf{H}^{T}),\\
&\mathbf{u} = \mathbf{u}_{(1)} + \mathbf{u}_{(2)}, \qquad \mathbf{H} = \nabla \mathbf{u}.
\end{aligned} \tag{2}$$

where, $\mathbf{u}$ is the displacement tensor, $\mathbf{n}_3$ is the outward unit normal vector to the plate surface, λ and μ are Lame's constants, $\mathscr{A}$, $\mathscr{B}$, and $\mathscr{C}$ denote the third-order elastic constants, and a black and bold letter denotes a tensor in this paper.

Consider primary wave propagation mode with frequency ω and corresponding wave number k excited at $x_1 = 0$. The primary wave solution can be written in the form:

$$\mathbf{u}_{(1)}(x_1, x_3, t) = \frac{1}{2}\mathbf{u}(x_3) e^{-i(kx_1 - \omega t)} + c.c. \tag{3}$$

where $c.c.$ denotes the complex conjugate. Then, the solution for the second harmonic wave can be written in the mode expansion form [12,13,15,17]:

$$\begin{aligned}
&\mathbf{v}_{(2)}(x_1, x_3, t) = \frac{1}{2}\sum_{n=1}^{\infty} a_n(x_1)\mathbf{v}_n(x_3) e^{-2i\omega t} + c.c.,\\
&a_n(x_1) = \frac{f_n}{4P_{nn}} \begin{cases} \dfrac{i(1 - e^{-i(k_n^* - 2k)x_1})}{(2k - k_n^*)} e^{-i2kx_1}, & \text{for } k_n^* \neq 2k \\ x_1 e^{-i2kx_1}, & \text{for } k_n^* = 2k \end{cases},\\
&f_n \equiv f_n^{surfce} + f_n^{volume}.
\end{aligned} \tag{4}$$

where, $\mathbf{v}_{(2)}(x_1, x_3, t) = \partial \mathbf{u}_{(2)}(x_1, x_3, t)/\partial t$; $a_n(x_1)$ is the amplitude of the n^{th} second harmonic mode $\mathbf{v}_n(x_3)$; k and k_n^* are the wave numbers of the primary and the n^{th} second harmonic modes, respectively; P_{nn} is the power flux carried by the n^{th} second harmonic mode; f_n^{volume} and f_n^{surfce} are power fluxes from the primary mode to the second harmonic mode through the volume and surface of the plate, respectively. As $k_n^* = 2k$ and $f_n \neq 0$, the amplitude of the secondary solution increases linearly in the direction of the propagation. Hence, the following two conditions must be satisfied for the internal resonance: (1) phase-velocity matching, $k_n^* = 2k$, and (2) non-zero power flux, $f_n \neq 0$.

According to Eq. (4), phase-velocity mismatching occurs if $k_n^* \neq 2k$. Therefore, setting

$$1 - e^{-i(k_n^* - 2k)x_1} = 0, \tag{5}$$

we can obtain:

$$x_N = \frac{2N\pi}{\left|k_n^* - 2k\right|} = \frac{2N\pi}{\left|\Delta k\right|},\ \Delta k = k_n^* - 2k.\ (N \text{ is a positive integer}) \tag{6}$$

Eqs. (5) and (6) show that the amplitude of the second harmonic changes with a distance period, L_n, where:

$$L_n = \frac{2\pi}{\left|\Delta k\right|}, \tag{7}$$

and the second harmonic wave has a maximum cumulative wave propagation distance, l_n

$$l_n = \frac{1}{2}L_n = \frac{\pi}{\left|\Delta k\right|} = \frac{\pi}{2\omega}\frac{c_p^{\omega}c_p^{2\omega}}{\left|c_p^{2\omega} - c_p^{\omega}\right|}, \tag{8}$$

where c_p^{ω} and $c_p^{2\omega}$ are the phase velocities of the fundamental and second harmonic waves, respectively. This phase-velocity mismatching is also called the π effect [12,16], which leads to limitations of the second harmonic accumulation for $k_n^* \neq 2k$ ($\Delta k \neq 0$ or $c_p^{2\omega} \neq c_p^{\omega}$).

The second harmonic wave is consistently generated when the non-zero power flux condition is satisfied. Due to dispersion, the second harmonic and fundamental waves have different phase velocities (which leads $\left|\Delta k\right|$ to non-zero). The newly-generated second harmonic and formerly-produced one interfere with each other [20]. Enhanced interference occurs when the phase difference varies in the interval [0, π). In contrast, interference attenuation occurs when the phase difference varies in the interval [π, 2π).

To overcome the interference attenuation and ensure the accumulation of the second harmonic generated during wave propagation, a π phase shift should be added to the newly-generated second harmonic at a wave propagation distance in the interval [$(2N-1)l_n$, $2Nl_n$), where N is a positive integer. Therefore, the following equations are derived:

$$a_n(x_1) = \frac{f_n}{4P_{nn}}\frac{i(1-e^{-i\Delta kx_1})}{(2k-k_n^*)}e^{-i2kx_1} = \frac{f_n}{4P_{nn}}\frac{i(e^{-i[2\pi-2N\pi]} - e^{-i(\Delta kx_1 - 2N\pi)})}{(2k-k_n^*)}e^{-i2kx_1}, \tag{9}$$

$$\begin{aligned} a_n(x_1) &= -[\frac{-f_n}{4P_{nn}}\frac{i(1-e^{-i\Delta kx_1})}{(2k-k_n^*)}] = \frac{-f_n}{4P_{nn}}\frac{i(-1+e^{-i\Delta kx_1})}{(2k-k_n^*)}e^{-i2kx_1} \\ &= \frac{-f_n}{4P_{nn}}\frac{i(-1-e^{-i\Delta k[x_1-(2N-1)l_n]})}{(2k-k_n^*)}e^{-i2kx_1} \\ &= \frac{-f_n}{4P_{nn}}\frac{i(e^{-i[2\pi-(2N-1)\pi]} - e^{-i[\Delta kx_1-(2N-1)\pi]})}{(2k-k_n^*)}e^{-i2kx_1}, \quad \text{for} \quad k_n^* \neq 2k. \end{aligned} \tag{10}$$

Eqs. (9) and (10) show that we can introduce a π phase shift of the newly-generated second harmonic at a wave propagation distance in the interval [$(2N-1)l_n$, $2Nl_n$) by changing the sign of f_n. Thus, interference enhancement of these second harmonics is achieved.

Note that changing the sign of f_n does not affect the sign of P_{nn}. Although the expression f_n is long and complex [12,13,15,17], it is unnecessary to write the explicit expression f_n. Thus, f_n can be expressed as a function of $\lambda, \mu, \mathscr{A}, \mathscr{B}, \mathscr{C}$ and $\mathbf{u}(x_1, x_3, t)$ (an odd function of $\lambda, \mu, \mathscr{A}, \mathscr{B}, \mathscr{C}$) as:

$$\begin{aligned} f_n &= f_n(\lambda, \mu, \mathscr{A}, \mathscr{B}, \mathscr{C}, \mathbf{u}(x_1, x_3, t)) = \\ & f_n(\sum(\alpha_\lambda \lambda + \alpha_\mu \mu + \alpha_{\mathscr{A}} \mathscr{A} + \alpha_{\mathscr{B}} \mathscr{B} + \alpha_{\mathscr{C}} \mathscr{C}) \cdot g(\mathbf{u}(x_1, x_3, t))), \end{aligned} \tag{11}$$

where, $\alpha_\lambda, \alpha_\mu, \alpha_{\mathscr{A}}, \alpha_{\mathscr{B}}$, and $\alpha_{\mathscr{C}}$ are the coefficients of , $\lambda, \mu, \mathscr{A}, \mathscr{B}$ and $\mathscr{C}$, respectively, and $g(\mathbf{u}(x_1, x_3, t))$ represents the function of $\mathbf{u}(x_1, x_3, t)$. Thus, one may change the sign of f_n in the following relationship:

$$-f_n = f_n(-\lambda, -\mu, -\mathscr{A}, -\mathscr{B}, -\mathscr{C}, \mathbf{u}(x_1, x_3, t)). \tag{12}$$

It is obvious that λ and μ are related to geometrical nonlinearity and $\mathscr{A}, \mathscr{B}$, and $\mathscr{C}$ are related to material nonlinearity, approximately. Eq. (12) can be decomposed as:

$$f_n = f_n^g(\lambda, \mu, \mathbf{u}(x_1, x_3, t)) + f_n^m(\mathscr{A}, \mathscr{B}, \mathscr{C}, \mathbf{u}(x_1, x_3, t)), \tag{13}$$

where function f_n^g denotes geometrical nonlinearity and function f_n^m represents material nonlinearity. To eliminate the influence of geometric nonlinearity, one may obtain an accumulation second harmonic generated mainly by material nonlinearity, through the following MQPM technique at a wave propagation distance interval $[(2N-1)l_n, 2Nl_n)$:

$$-f_n^m = f_n^m(-\mathscr{A}, -\mathscr{B}, -\mathscr{C}, \mathbf{u}(x_1, x_3, t)). \tag{14}$$

To obtain the analytical results, assuming that the Lamb wave is transmitted at the location $x_1 = 0$, the amplitude of the second harmonic generated by material nonlinearities can be expressed as [19]:

$$\begin{aligned} a_n^m(x_1) &= \frac{f_n^m}{4P_{nn}} \frac{c_p^\omega c_p^{2\omega}}{\omega(c_p^{2\omega} - c_p^\omega)} \cdot \sin\left(\frac{\omega(c_p^{2\omega} - c_p^\omega)}{c_p^\omega c_p^{2\omega}} x_1\right), \quad \text{(without MQPM)} \\ E\left(a_n^m(x_1)\right) &\propto (a_n^m(x_1))^2, \end{aligned} \tag{15}$$

where E represents the energy of the second harmonic. Setting the energy peak amplitude of $E\left(a_n^m(x_1)\right)$ as $E_{\max}$, and correlating with Eqs (5)-(15), one can generate:

$$\begin{aligned} E\left(\overline{a_n^m(x_1)}\right) \propto & \begin{cases} ME_{\max} + (-1)^M E\left(a_n^m(x_1)\right), & \text{for } M \text{ is even} \\ (M+1)E_{\max} + (-1)^M E\left(a_n^m(x_1)\right), & \text{for } M \text{ is odd} \end{cases} \quad \text{(with MQPM)} \\ & \text{and } M = [x_1 / l_n], \end{aligned} \tag{16}$$

where $\overline{a_n^m(x_1)}$ denotes the amplitude of the second harmonic with MQPM and $[\bullet]$ represents the bracket function.

3 SIMULATION

As shown in Fig. 1, according to the phase dispersion curves of symmetric mode Lamb waves in an aluminum plate (thickness 2*h*=2 mm) with the material properties in Table 1, the corresponding phase velocities at $f \cdot d$ = 0.2 MHz×mm and 0.4 MHz×mm can be obtained as 5434.0 m/s and 5391.0 m/s, respectively. Considering Eq. (8), the second harmonic maximum cumulative propagation distance l_n is around 700 mm. MQPM can be achieved by periodically changing the sign of the third-order elastic constants at the wave propagation distance interval $[(2N-1)l_n, 2Nl_n)$.

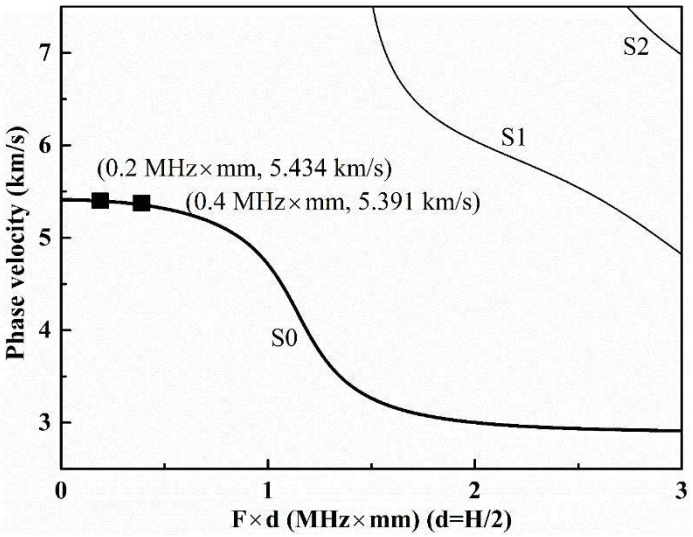

Figure 1: The phase dispersion curves of symmetric Lamb wave modes in an aluminum plate with thickness *H*=2*d*=2*h*=2mm. Page layout

To verify the theoretical results, a commercial FEM software, *i.e.*, COMSOL [16,18], is adopted. To obtain adequate accuracy and high efficiency, a second-order rectangular element type is used, and the maximum element size and time step are calculated according to the literature [16]

$$\Delta I = \lambda_{\min} / 20, \tag{27}$$

$$\Delta t = 1/(20 f_{\max}), \tag{28}$$

where ΔI is the element size (0.5 mm), Δt is the time step ($5x10^{-8}$ s), $\lambda_{\min}$ and $f_{\max}$ are the shortest wavelength and highest frequency of interest, respectively.

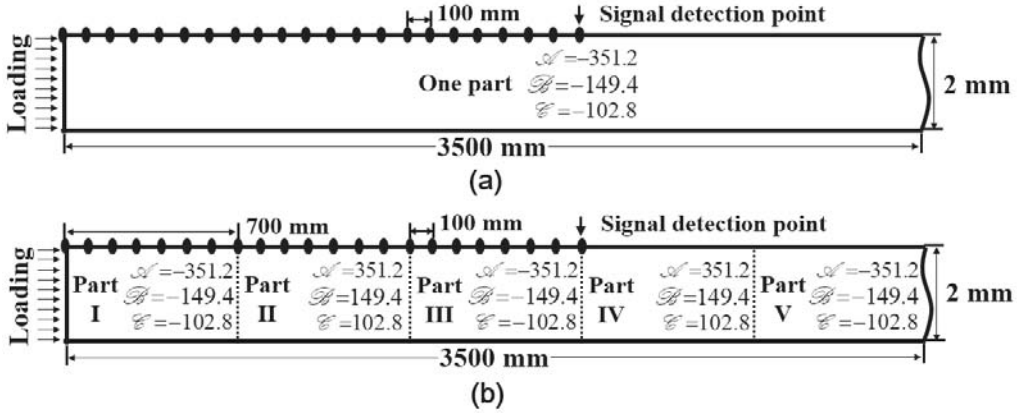

Figure 2: The 1-D Al-7075-T651 plate model. The material properties are determined from Table 1. (a) The reference model contains one part. (b) The periodic model includes five parts. The sign of the third-order elastic constants of Parts II and IV are opposite to those of Parts I, III, and V.

Table 1: Material properties of Al-7075-T651 (in one part or in Part I, III, and V)

ρ (kg/m^3)	λ (*GPa*)	μ (*GPa*)	$\mathscr{A}$ (*GPa*)	$\mathscr{B}$(*GPa*)	$\mathscr{C}$ (*GPa*)
2810	70.3	26.96	-351.2	-149.4	-102.8

As shown in Fig. 2, two simulation models are established. Fig. 2(a) shows the reference model (without MQPM) containing only one part whose material properties are the same as those in Table 1. To verify that the second harmonic can be steadily accumulated, another periodic five-part model (with MQPM) is built. As shown in Fig. 2(b) and the upper of Fig. 3, the sign of the third-order elastic constants of Parts II and IV are opposite to those of Parts I, III, and V. The widths of Parts I, II, III, and IV are set to l_n=700 mm. The length of the plate with an aluminum Al-7075-T651 is set to be 3500 mm, which is long enough to eliminate the reflected wave. The low reflection boundary condition is applied to the right end during the simulation, and the upper and lower surfaces of the plate are free. Prescribed uniform pressure loading is actuated on the left end of the plate to excite the desired primary S0 mode Lamb waves. The actuating function of the excitation signal is described as: $x(t) = 0.5P\sin(2\pi ft)(1-\cos(2\pi ft/N))$, where f (=200 kHz) is the central frequency, N (=10) is the number of sinusoidal cycles in the tone burst, and P (=10 MPa) is the amplitude of tone-burst. Twenty-two signal detection points are considered from 0 mm to 2100 mm with an increment of 100 mm from the left of the model.

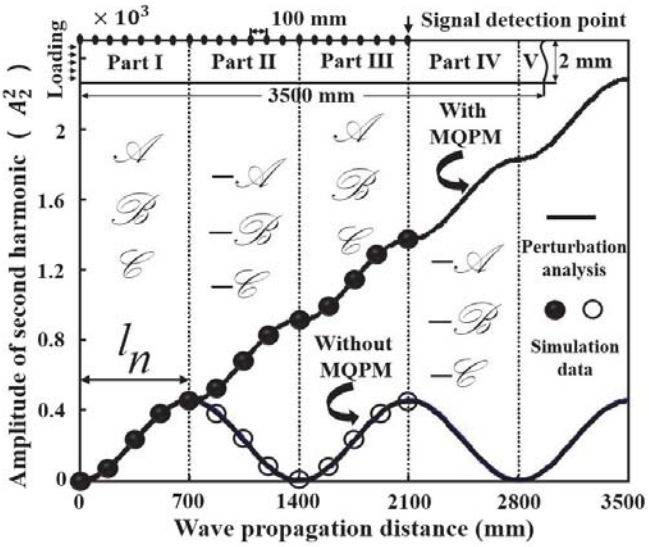

Figure 3: The 1-D periodic Al-7075-T651 plate consisting of sub-domains with alternate third-order elastic constants $\mathscr{A}$, $\mathscr{B}$ and $\mathscr{C}$. The dots and circles represent the simulation data and the solid lines denote the perturbation analysis results. The MQPM technique causes the curve and dots monotonically increase. Without the MQPM technique, the curve and circles indicate that the energy of the second harmonic increase with wave propagation distance in the form of a sine function and exhibit a maximum cumulative propagation distance of 700 mm due to phase mismatching. Thus, the MQPM technique can be achieved by periodically changing the sign of the third-order elastic constants at the wave propagation distance interval $[(2N\text{-}1)\, l_n, 2Nl_n)$. The energy carried by the second harmonic can be monotonically enhanced.

Analytical results and the corresponding numerical simulation results for the second harmonic intensity in the form of energy are both plotted in Fig. 3. The lower curve represents the theoretical results without MQPM, which is in accordance with results reported in previous studies [12,18]. The amplitudes of the second harmonic increase with the wave propagation distance in the form of a sine function and exhibit a maximum cumulative propagation distance due to the π effect caused by the deterioration of phase-velocity matching conditions. The upper curve denotes the analytical results with MQPM, which shows that the second harmonic can be continuously accumulated. The circles represent the simulation results of the model without MQPM, and the dots denote the numerical results of the model with MQPM. It can be observed that the results of the simulation and perturbation analysis are consistent with one another. Note that when different frequencies of excitation signals are used, such as 100, 300, and 400 kHz, the energy change tendencies of the second harmonic in Fig. 3 are similar. Thus, the energy carried by the second harmonic can monotonically increase through MQPM.

To practically apply the MQPM technique, the key concern is to realize the sign change of the third-order elastic constants (TOE) $\mathscr{A}$, $\mathscr{B}$, and $\mathscr{C}$ in Parts II and IV. Basically, $\mathscr{A}$, $\mathscr{B}$, and $\mathscr{C}$ are the inherent material properties to evaluate the material nonlinearity of the medium. Considering one-dimensional longitudinal waves for simplicity, the stress-strain

relationship in a nonlinear solid can be expressed, with a second-order approximation, as follows [16,21]

$$\sigma=E^*\varepsilon(1+\beta\varepsilon). \tag{29}$$

where σ , ε and E^* denote the stress, strain, and Young's modulus of the material, respectively, while β is the nonlinear parameter related to the second derivative of the stress-strain curve. For an isotropic material, β can be defined as [16,21]

$$\beta=-[3+(2\mathscr{A}+6\mathscr{B}+2\mathscr{C})/E^*]. \tag{30}$$

The negative three-order elastic coefficients (NTOE) imply that the second derivative of the stress-strain curve is positive (β positive), while the positive three-order elastic coefficients (PTOE) mean that the second derivative of the stress-strain curve is negative (β negative). For a monotonically increasing stress-strain curve, NTOE means that this curve is of a lower convex shape, while for PTOE, it is of an upper convex shape.

Generally, there may be two methods to change the TOE, at least. For a composite material plate (ignoring the band gap [22] for simplicity), the sign change of TOE can be realized by a composite plate periodically consisting of positive β, *i.e.*, material A (β(Dural) =11.8 [23]) and negative β, *i.e.*, material B (β(Silica)= – 7.4 [23]) with the same width (here, l_n=700 mm). For a single material plate, the sign change of TOE can be realized by periodically applying a uniform tension force (much easier for soft materials [24]). Here, for example, a proper uniform tension force applied on Parts II and IV is recommended. In this case, the key issue is that the tension force changes the material's stress-strain curve from a lower convex shape into an upper convex shape. Of course, the sign change of TOE looks difficult (easy for soft materials) at present. However, it is not impossible at all. Further studies are needed on this issue.

4 CONCLUSIONS

For any excitation frequency, the monotonic growth of the second harmonic Lamb wave is possible even when the phase-velocity matching conditions are not exactly satisfied using the MQPM technique. Achieving this method is relatively easy in theory and simulation. However, the MQPM technique needs to change the sign of the third-order elastic constants, which may be difficult (much easier for soft materials) to realize in practice. Further studies and improvements are needed for this issue. Despite some difficulties at the experimental stage, the self-consistent theoretical results are interesting and have a certain scientific significance. Based on MQPM, ultrasonic frequency converters might be invented in the future.

In summary, we present theoretical analysis and simulation results to demonstrate that the enhancement of the second harmonic Lamb wave energy is possible (in the whole frequency bandwidth) even when the phase-velocity matching conditions are not exactly satisfied using the MQPM technique. Experimental studies will be focused on in the future.

FUNDING

This work was supported by the Chinese National Natural Science Fund [grant number 12204076], the Natural Science Foundation of Chongqing CSTC [grant number 2022NSCQ-MSX0417], and the Doctoral Program Fund of Chongqing Industry Polytechnic College [grant number 2022G2YBS2K3-18].

REFERENCES

[1] J.A. Armstrong, Interactions between light waves in a nonlinear dielectric, *Physical Review Letters*, 1962. 127: pp. 1918-1939.
[2] S.N. Zhu, et al., Quasi-phase-matched third-harmonic generation in a quasi-periodic optical superlattice, *Science*, 1997. 278: pp. 843-846.
[3] A. E. Gibson, , Coherent soft X-ray generation in the water window with quasi-phase matching, *Science*, 2003. 302: pp. 95-98.
[4] M. Baudrier-Raybaut, et al., Random quasi-phase-matching in bulk polycrystalline isotropic nonlinear materials, *Nature*, 2004. 432: pp. 374-376.
[5] A. Bahabad, et al., Quasi-phase-matching of momentum and energy in nonlinear optical processes, *Nature Photon*, 2010. 4: pp. 571-575.
[6] B.Q. Chen, et al., High-efficiency broadband high-harmonic generation from a single quasi-phase-matching nonlinear crystal, *Physical Review Letters*, 2015. 115: pp. 083902.
[7] S. Kroesen, et al., Monolithic fabrication of quasi phase-matched waveguides by femtosecond laser structuring the $\chi(2)$ nonlinearity, *Applied Physics Letters*, 2015. 107: pp. 1-5.
[8] A. Billat, et al., Large second harmonic generation enhancement in SiN waveguides by all-optically induced quasi phase matching, *Nature Communications*, 2017. 8: pp. 1016.
[9] G.X. Cui, et al., Quasi-phase-matched second harmonic generation of long-range surface plasmon polaritons, *Optics Express*, 2018. 26: pp. 4194.
[10] M. Deng, Cumulative second-harmonic generation of Lamb-mode propagation in a solid plate, *Journal of Applied Physics*, 1999. 85: pp. 3051-3058.
[11] M. Deng, Analysis of second-harmonic generation of Lamb modes using a modal analysis approach, *Journal of Applied Physics*, 2003. 94: pp. 4152-4159.
[12] W.J.N.D. Lima, M.F. Hamilton, Finite-amplitude waves in isotropic elastic plates, *Journal of Sound and Vibration*, 2003. 265: pp. 819-839.
[13] A. Srivastava, F. L. D. Scalea, On the existence of antisymmetric or symmetric Lamb waves at nonlinear higher harmonics, *Journal of Sound and Vibration*, 2009. 323: pp. 932-943.
[14] K.H. Matlack, et al., Experimental characterization of efficient second harmonic generation of Lamb wave modes in a nonlinear elastic isotropic plate, *Journal of Applied Physics*, 2011. 109: pp. 14905.
[15] V. K. Chillara, C.J. Lissenden, Interaction of guided wave modes in isotropic weakly nonlinear elastic plates: Higher harmonic generation, *Journal of Applied Physics*, 2012. 111: pp. 124901-124909.

[16] V. K. Chillara, C.J. Lissenden, Nonlinear guided waves in plates: A numerical perspective, *Ultrasonics*, 2014. 54: pp. 1553-1558.
[17] X.Q. Sun, et al., Interaction of Lamb wave modes with weak material nonlinearity: Generation of symmetric zero-frequency mode, *Sensors*, 2018. 18: pp. 2451-2470.
[18] X. Wan, et al., Analytical and numerical studies of approximate phase velocity matching based nonlinear S0 mode Lamb waves for the detection of evenly distributed microstructural changes, *Smart Materials and Structures*, 2016. 25: pp. 045023.
[19] Y. Ishii, et al., Non-collinear interaction of guided elastic waves in an isotropic plate, *Journal of Sound and Vibration*, 2018. 419: pp. 390-404.
[20] M. Deng, et al., Experimental observation of cumulative second-harmonic generation of Lamb-wave propagation in an elastic plate, *Journal of Physics D: Applied Physics*, 2005. 38: pp. 344-353.
[21] Y. Shen, V. Giurgiutiu, Predictive simulation of nonlinear ultrasonics, *The International Society for Optical Engineering*, 2012.
[22] A. Wautier, B.B. Guzina, On the second-order homogenization of wave motion in periodic media and the sound of a chessboard, *Journal of the Mechanics and Physics of Solids*, 2015. 78: pp. 382-414.
[23] X. Jacob, et al., Experimental study of the acoustic radiation strain in solids, *Applied Physics Letters*, 2006, 88: pp. 528.
[24] G.Y. Li, et al., Guided waves in pre-stressed hyperelastic plates and tubes: Application to the ultrasound elastography of thin-walled soft materials, *Journal of the Mechanics and Physics of Solids*, 2017. 102: pp. 67-79.